

Simulation of Infrared Spectra for β -Hairpin Peptides Stabilized by an Aib-Gly Turn Sequence: Correlation between Conformational Fluctuation and Vibrational Coupling

Joohyun Kim,[†] Rong Huang,[†] Jan Kubelka,^{†,§} Petr Bouř,[‡] and Timothy A. Keiderling^{*,†}

Department of Chemistry, University of Illinois at Chicago, 845 West Taylor Street, Chicago, Illinois 60607-7061, and Institute for Organic Chemistry and Biochemistry, Academy of Science of the Czech Republic, Flemingovo nam. 2, 16610, Praha 6, Czech Republic

Received: June 28, 2006; In Final Form: August 31, 2006

Vibrational spectra of a 12-residue β -hairpin peptide, RYVEVBGKKILQ (HBG), stabilized by an Aib-Gly turn sequence (B = Aib) were investigated theoretically using a combination of molecular dynamics (MD) and density functional theory (DFT) calculations. Selected conformations of HBG were extracted from a classical MD trajectory and used for spectral simulations. DFT calculations, based on the Cartesian coordinate spectral property transfer protocol, were carried out for peptide structures in which all residues are replaced with Ala, except for the Aib and Gly residues, but the backbone (ϕ, ψ, ω) structure of the original configuration is retained. The simulations provide a basis for interpretation of the HBG amide I infrared spectra in terms of structural variables such as detailed secondary structure and thermal conformational fluctuation as well as vibrational coupling as indicated by spectra of ^{13}C isotope-labeled variants. The characteristic amide I band shape of such small β -hairpin peptides appears to arise from the structure of the short antiparallel β -sheet strands. The role of structural parameter fluctuation in vibrational coupling is evaluated by comparison of DFT-derived amide coupling constants for selected configurations and from transition dipole coupling calculations of coupling parameters between ^{13}C isotopically labeled residues for a MD-derived ensemble of configurations. Calculated results were compared with the experimentally obtained spectra for several ^{13}C isotope-labeled peptides of this sequence.

Introduction

Theoretical and computational methods for simulating vibrational spectra have significantly advanced during the past decade due to successes with ab initio molecular orbital (MO) calculations facilitated by cheaper computing costs and improved algorithms particularly employing density functional theory (DFT) methods.^{1–4} At the same time, demands for interpreting vibrational spectra of peptides and proteins in terms of detailed structural, energetic (force field), and dynamic perspectives have been growing as new experimental data become available.^{5–7} Due to their relatively high accuracy and efficiency, DFT simulations of vibrational spectra have increasingly important roles for structural studies on biologically relevant systems.

Nonetheless, simulation of vibrational spectra is still challenging if one uses quantum mechanical (QM) methods and larger basis sets to study sizable peptides of biological relevance. Vibrational spectra could be calculated through an analysis of an ensemble-averaged time-dependent correlation function.^{8–11} However, this approach is not generally applicable, especially if ab initio calculations are necessary, due to the high computing cost. Rather, simulation of spectra is carried out by calculating harmonic frequencies for unique quantum mechanically optimized structures, and then a spectral profile is created by giving the components a natural line width and summing them. While employing a hybrid functional such as B3LYP for DFT

calculation and including diffuse functions in the basis set may be desirable for precise simulations of complete oligopeptide vibrational spectra,³ we have found that use of a pure density functional (i.e., not containing the Hartree–Fock exchange term) such as BPW91 and a polarized split valence basis such as 6-31G** is computationally more efficient and yields acceptable simulation of the higher-frequency, relatively local amide modes, which are the focus of most IR and Raman peptide studies.^{12,13}

Typically only a small number of representative structures are used for simulation, such as those obtained experimentally by X-ray diffraction or NMR studies. Recently, to overcome the limitations of employing a minimal number of configurations, several approaches have appeared in the literature based on QM/molecular dynamics (MD) calculations for simple systems.^{14–19} In addition, simulating the effects of solvating the molecular system of interest represents another major challenge, but several potential methods have appeared.^{14,15,18,20,21} In particular, in our studies, the best predictions of experimental amide I frequencies and band shapes have used explicit consideration of hydrogen-bonded water molecules, but this is very computationally intensive.²⁰ The value of considering the solvent effects in spectral simulation depends on the goals of the computation. Solvent shifts from vacuum results have been shown to be predictable for many structures, which suggests that empirical corrections should be sufficient.^{14,15,22}

In this study we examine the impact of the dynamical conformational fluctuation on the vibrational spectral properties for a small, relatively flexible β -hairpin-forming peptide, whose turn is stabilized by an Aib-Gly turn sequence (Aib is amino-isobutyric acid or α, α -dimethyl glycine, an α -substituted, non-

* Author to whom correspondence should be addressed. E-mail: tak@uic.edu.

[†] University of Illinois at Chicago.

[‡] Academy of Science of the Czech Republic.

[§] Current address: Department of Chemistry, University of Wyoming, 1000 E. University Ave., Laramie, WY 82071.

proteinic residue).²³ Interest in such a small β -hairpin stems from the goals of understanding fast time scale folding–unfolding dynamics and explaining the stability of this minimal antiparallel β -sheet model.^{24–28} Previous hairpin studies have included vibrational spectra, but DFT-level calculations for this size of peptide are demanding.^{27,29–38} A critical complication in such spectral simulations is the lack of regularity in hairpin structures, which makes our previous propagation methods for property tensor transfer less applicable.^{13,31} Instead, our modified substructure-transfer protocol was tested and applied for DFT-level spectral simulation.³¹ Selected structures that are sampled from MD trajectories were used for the DFT calculations. Considering the difficulty in computing QM spectra for such hairpins, we limited DFT-level calculations to only a few structures chosen to exemplify conformational variation along the MD trajectory. These examples are selected for diversity, not to be complete or represent some average over a trajectory. They illustrate spectral variances that characterize folding–unfolding in temperature-dependent IR spectra as developed through the pattern of amide I spectral changes obtained with parameter-free, DFT-level calculations.

Additionally we modeled the impact of conformational fluctuation on IR bands arising from specific ¹³C isotope-labeled amide C=O groups. Site-specific coupling in these amide I bands has stimulated their application for structural determination in biophysical studies such as protein folding, protein–ligand interactions, and protein–membrane interactions.^{39–53} Selected cross-strand coupling in β -hairpins, spectrally isolated by labeling, provides a means of using IR to site-specifically probe the unfolding mechanism. At the DFT level, ¹³C amide I bands were simulated for the selected structures by substituting ¹³C atoms into specific amide C=O groups. Last, to examine the role of thermally induced conformational fluctuations, vibrational coupling between pairs of isotope-labeled amide groups was investigated by use of the transition dipole coupling (TDC) model for an ensemble of configurations obtained from MD.^{6,54,55}

Calculation Details

Peptide Model and MD Simulation for Configuration Sampling. The 12-residue peptide structure used for the MD simulation has the same sequence, NH₃-RYVEVBGKK-ILQ-NH₂ (B = Aib), as the peptide used for our recently reported experimental spectroscopic studies.²³ This is a modification of Gellman's 12-residue hairpin sequence⁵⁶ that we designate as HBG.²³ In Figure 1, a schematic of a fully folded state of the peptide is presented with our notation for the five possible hydrogen-bond pairs. For example, H_A represents the hydrogen-bond distance between O of Val5 and N of Lys8. Each carbonyl group is numbered according to its relative position from the turn, with the N-terminal residues being negative and the C-terminal residues being positive. This numbering scheme will be used for the notation of coordinate spectral property transfer (CSPT) fragments as well as to indicate ¹³C-labeled amide groups.

MD simulations and analyses were performed with the Gromacs package (<http://www.gromacs.org>), and specific analyses of the results were performed by our Python scripts (<http://www.python.org>).⁵⁷ A cubic simulation box of approximately 3.0 nm on a side was used to contain one peptide and approximately 1500 water molecules. The OPLS-AA all atomic force field was employed, with the SPC model for water.^{58,59} All bonds are constrained with the LINCS algorithm. All simulations were performed in the NVT ensemble, with the

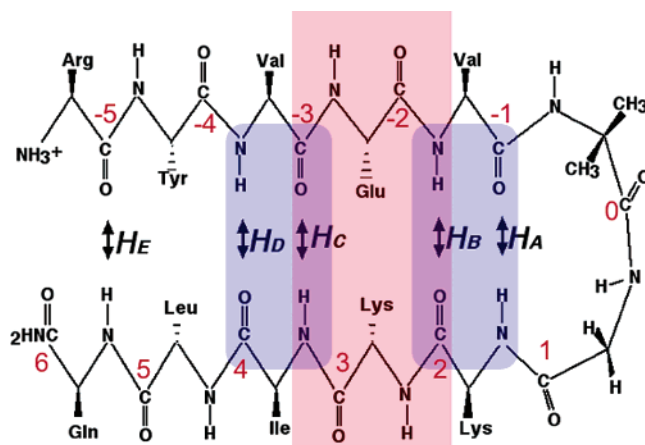


Figure 1. Schematic diagram of HBG cross-strand interactions in the fully folded state including notations for hydrogen bonds, amide groups, and isotopically labeled variants.

temperature being controlled by a Berendsen thermostat with a coupling time constant of 0.1 ps. Long-range cutoffs of 1.0 nm were employed. The water box equilibrated in $T = 297$ K and $p = 1$ atm was used for solvating the peptide. MD simulations were carried out for several independent trajectories with various starting structures and temperatures spanning 300–500 K and reaching many tens up to 100 ns in length. The initial configuration was a model folded structure, but many other trajectories were restarted with configurations obtained from previous trajectories. Such extensive simulation is expected to yield characteristics of the configuration space for the folded state as well as unfolding–refolding dynamical processes. Among these trajectories, MD runs at 300 and 400 K were chosen for analyzing the conformational fluctuation of the folded state and for sampling structures for the spectral simulation.

Amide I IR Spectra Simulation. DFT Calculations. Our approach employing DFT-level parameter-based simulation of vibrational spectra of sizable peptides is based on transferring Cartesian coordinate based properties such as force field (FF), atomic polar tensor (APT), and atomic axial tensor (AAT) from DFT calculations on smaller model oligomer systems onto large molecules of interest.^{13,60} The selected small models share structural characteristics, such as (ϕ, ψ) torsions, with the entire peptide and thus can be termed “substructures” or segments to avoid any confusion with the term “fragment”, which has been used to designate much smaller structures computed in other approaches.^{54,61}

All DFT-level calculations, geometry optimizations, and frequency calculations were performed with Gaussian 98 or 03 at the BPW91/6-31G** level, following methods established in our previous peptide publications.^{13,62} Calculated spectral properties of each substructure are transferred to the target molecular system by means of in-house programs.⁶⁰

Model Structures. Peptide conformations were derived from 300 K MD trajectories for HBG in water. The C-terminal amide group was removed, since its impact on the spectral properties of interest in this study should be minimal (it can have no cross-strand hydrogen bond), resulting in structures with 11 amides. The N- and C-termini are capped with Ac- (CH₃-CO-) and -N-Me (-NH-CH₃) groups, respectively. For DFT modeling the backbone structure derived from these MD-derived conformations is retained, but all residues are replaced with Ala, except for Aib and Gly, to reduce the computational load. This is (at least partially) justified by many previous theoretical and

experimental studies indicating that major peptide and protein IR and VCD amide absorbance bands (I and II) arise from modes localized on the backbone.

From our previous studies,³¹ the minimal number of segments for the folded state β -hairpin peptide structure was chosen to be three: one for the turn region, another from the middle of both strands, and the final one that includes the end groups. The substructure for the turn was chosen to have five amides, and the two other substructures have six amides (three in each strand). All substructures are capped with Ac- and -N-Me groups at the N- and C-termini, respectively. According to our numbering scheme for the amide groups (Figure 1), a 5-amide size segment containing the turn from the amide group at -2 to the amide group at 2 will be designated as [-2:2], a 6-amide size segment containing the -4, -3, -2, 4, 3, 2 amide groups will be [-4:-2, 4:2], and another 6-amide segment will be [-5:-3, 5:3]. For the extended conformation representing the unfolded structure, three distorted strands were used: N-terminus 6-amides [-5:0], middle 6-amides, [-3:2], and C-terminus 6-amides, [1:6].

Isotope-Labeled Spectra Calculations. The three isotope-labeled variants that we will discuss here are each substituted with ¹³C on a different pair of cross-strand coupled amide C=O groups. According to our numbering scheme, the labeled C=O groups are -3 and 2 (for the labeled β -hairpin denoted as HGB1), -3 and 4 (denoted as HGB2), and -1 and 2 (HGB3). Simulations of spectra for isotopically substituted hairpin models were obtained with the same transferred DFT parameters by substituting the appropriate atomic masses. To provide an alternative point of view that could be applied to a larger ensemble of structures, the TDC approximation^{6,55,63,64} was used to compute dipolar coupling constants between the labeled amide groups indicated by HGB1, HGB2, and HGB3 for an ensemble of structures derived from two MD runs at 300 and 400 K (Figure 2). Torii and Tasumi's previously reported dipole parameters were used for TDC calculations on these ensembles of labeled hairpins.^{55,64}

Results

Thermal Conformational Fluctuation of HGB. From MD trajectories, characteristics of the structural fluctuation of HGB in water can be envisaged, enabling selection of conformations for spectral simulation. Also, information about the ensemble-averaged hydrated peptide structure can be obtained, which is useful for determining the solvent effects on spectra.

The thermal conformational fluctuation in the folded state was analyzed with two MD trajectories simulated at 300 and 400 K. Their time evolutions, monitored by five hydrogen-bond distances as defined in Figure 1, are shown in Figures 2a and 2b, where H_E at 400 K is not shown due to its much higher level of fluctuations reflecting the completely frayed ends. The distributions of corresponding hydrogen-bond distances at H_A , H_B , H_C , and H_D are shown in Figures 2c and 2d, for $T = 300$ and 400 K, respectively. For calculation of a distribution of hydrogen-bond distances, configurations were sampled at a 10 ps interval. Since only folded configurations were considered, 1000 configurations were used for the 300 K run, and 700 configurations for the 400 K run.

The most notable aspect of Figures 2a and 2b is that the short β -strand region, comprising the residues that form H_B , H_C , and H_D , demonstrates overall structural stability during these trajectories. The H_B and H_C distances are the most stable and show very similar fluctuation distributions at 300–400 K, while the H_D distance shows more fluctuation at the higher temper-

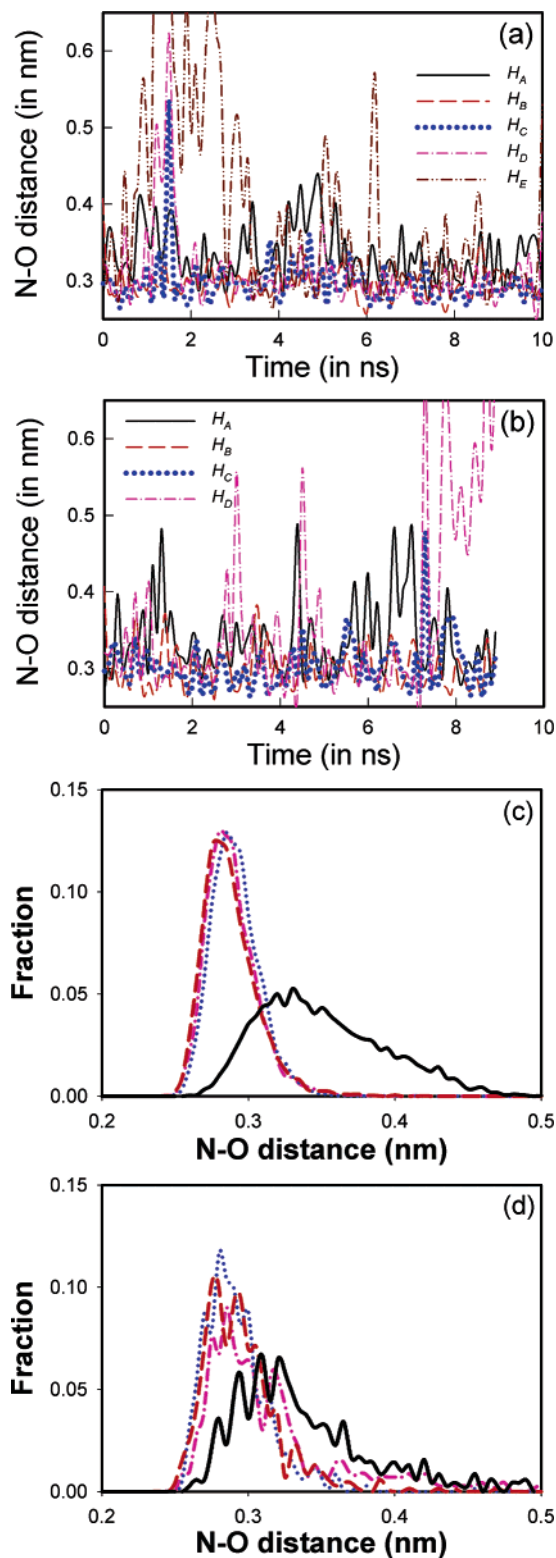


Figure 2. Thermal conformational fluctuation of HGB. Two trajectories at 300 and 400 K are displayed. (a) Time evolutions of five hydrogen-bond distances (300 K). (b) Time evolutions of four hydrogen-bond distances (400 K). (c) Normalized distributions of hydrogen-bond distances at H_A , H_B , H_C , and H_D (300 K). (d) Normalized distributions of hydrogen-bond distance (400 K). The solid line (black) is for H_A , the long dashed line (red) is for H_B , the dotted line (blue) is for H_C , the dash-dotted line (pink) is for H_D , and the dash-dot-dotted line (brown, only in part a) is for H_E , respectively. The distributions in parts c and d are obtained only for folded configurations sampled over the trajectories shown in parts a and b, respectively. The initial system configurations of these trajectories were prepared after several nanosecond runs starting from a model folded structure.

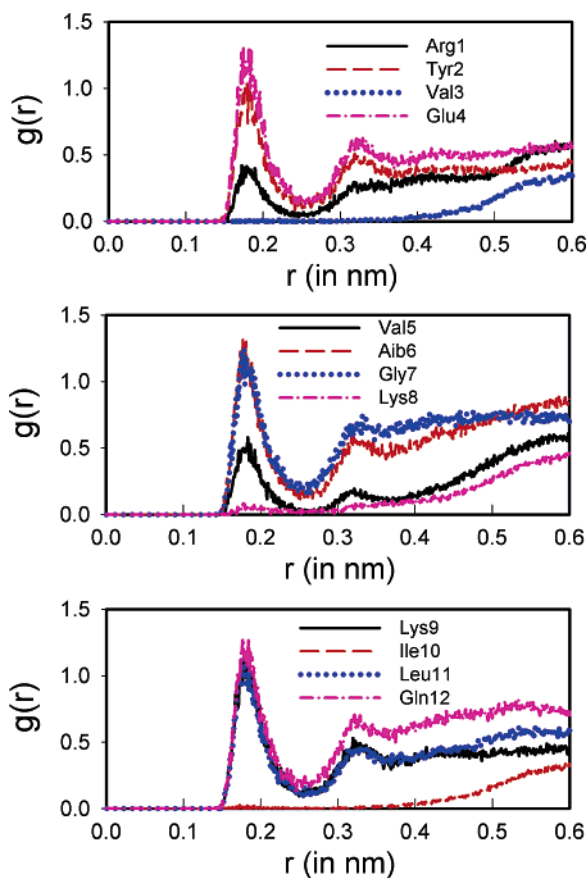


Figure 3. Hydration structure of 12 amide groups in HBG at 300 K. The radial distribution function (RDF), $g(r)$, is obtained for O in each amide C=O and the hydrogens in all the water molecules.

ature. This suggests that the hairpin can encompass a more distorted structure at higher temperatures, essentially being more frayed toward the ends of the strands, while its core residues maintain their overall folded, or at least compact, character. As expected, H_E shows the most significant fluctuations at both temperatures.^{35,65} More interestingly, fluctuation at H_A is significant compared to H_B and H_C , even comparable to H_D . Such turn instability has been observed by other workers with different β -hairpin models.^{65–67} While the turn structure has noticeable fluctuation, it maintains the qualitative characteristics of a type I β -turn that is apparently locked in by the Aib-Gly sequence.⁶⁸ These fluctuations are also reflected in the contact distance distributions (Figures 2c and 2d) where H_A is much broader than H_B and H_C .

Another important observation is related to the hydration structure. The radial distribution function between the O of each amide C=O and the hydrogens of all the water molecules was calculated at 300 K (Figure 3). Unlike carbonyl groups exposed to solvent, carbonyl groups participating in an interstrand hydrogen bond are generally shielded from water molecules due to the packing of side chains along the cross-strand region that contains the amide as shown in the radial distributions of water relative to each amide C=O. Particularly, at 300 K, carbonyl groups involved in H_B , H_C , and H_D (Lys8, Val3, and Ile10) are well-protected due to the presence of hydrophobic interactions as well as the stability of the backbone structure. On the contrary, due to fraying ends, the carbonyl group at H_E (Arg1) is only partially protected. Even the carbonyl group at H_A (Val5) is partially exposed to water, due to both significant fluctuation and the highly distorted turn structure. Thus, our MD results suggest that the short β -strand region characterized by H_B , H_C ,

and H_D is the characteristic structural element of the β -hairpin and is likely to be a common element in spectral characterization for stable hairpins. In contrast, the ends of the individual strands and, interestingly, the turn segment are more dynamical in nature.

9-Amide Fragment Calculation. To investigate the effects of the structural flexibility on the vibrational spectra we transfer to the target peptides spectral parameters computed for shorter segments, which yields virtually DFT-level descriptions of local vibrational characteristics in much larger structures. To test the reliability of the segment vibrational parameter transfer implementation used for this study, we compared the results for a full DFT calculation of a 9-amide size hairpin with those of parameter transfer from subcomponent segments. The 9-amide conformation is taken from a well-folded structure obtained from our MD trajectory, which will be used later for an 11-amide transferred calculation representing the full peptide. According to our numbering scheme, the truncated 9-amide hairpin includes amides from -4 to 4 capped with $-NMe$ and $Ac-$ on the C- and N-termini, respectively, and thus we designate it as a $[-4:4]$ hairpin. The size of this peptide is chosen to contain the turn region and most of the cross-strand β -sheet-forming residues that consist of three successive amide groups in each strand. While the cross-strand β -sheet region might extend to the end groups including the pair H_E , as described with MD trajectories in Figure 2, our computed folded configurations of HGB have end groups that are frayed even at low temperature. The 9-amide peptide was chosen for computational efficiency, but the result also helps to establish the origin of the characteristic spectral patterns for β -hairpin peptides. The segmentation scheme adopted for the simulation of the IR spectra for the same 9-amide $[-4:4]$ peptide by transfer uses a 5-amide turn, or $[-2:2]$, and a 6-amide double strand, or $[-4:-2,2:4]$.

The amide I IR spectra for the $[-4:4]$ hairpin resulting from the transfer and the full DFT calculations, respectively, are shown in Figures 4a and 4b. The line shapes shown are the result of summing 20 cm^{-1} full width at half-maximum Lorentzian line shapes scaled to the dipole strength D and positioned at the calculated frequencies. Comparison of the line shapes demonstrates the qualitative utility of the transfer method. Both show the low-frequency, intense peak calculated at $\sim 1685\text{ cm}^{-1}$ as well as the exciton split overall band shape due to the dispersion of the weaker modes up to $\sim 1730\text{ cm}^{-1}$. (These frequencies represent the vacuum DFT FF and are uncorrected for the expected error due to neglect of solvent.^{12,20,31}) Details of individual mode intensities and frequency positions do differ between the DFT- and the transfer-based calculation, but these tend to be issues of relative intensity or reordering of weak features and have only a modest impact on the overall, observable IR band profile. If probed using differential techniques, such as vibrational circular dichroism (VCD), then these small mode reorderings could have a larger effect on the observed band shape, due to the sign character of each transition. However, in this particular example the major impact on VCD is one of bandwidth (the DFT pattern is narrower) rather than shape (results not shown). That the higher-energy modes are more intense and less disperse for the segment-based transfer calculations may be due to end effects causing added dipole moment in these modes and to reduced exciton coupling in the short strands.

We introduce a similarity measure between normal modes resulting from these two calculations to provide a more quantitative method comparison and test of the transfer method. The similarity of two different eigenvectors, i.e., vibrational

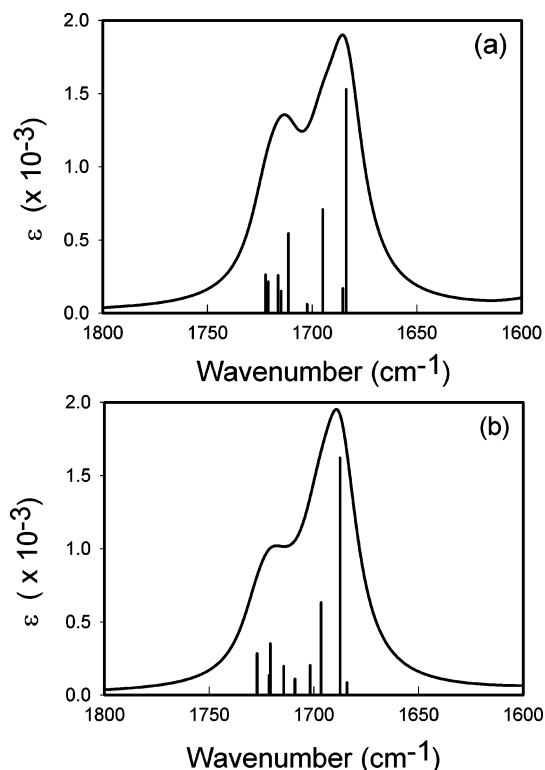


Figure 4. Amide I IR spectra of the 9-amide β -hairpin model. (a) Simulated spectra by the CSPT and (b) simulated spectra with the direct DFT.

modes, can be expressed as a scalar product

$$P_{A,B_j} = \left| \sum_{\lambda=1 \dots \text{NAT}, \alpha=1 \dots 3} S_{\lambda\alpha}^{I,A} S_{\lambda\alpha}^{J,B} \right| \quad (1)$$

where $S_{\lambda\alpha}^{I,A}$ is the S matrix atomic displacement vector for atom λ along coordinate α , in normal mode I or J , from a calculation A or B . For identical modes we obtain $P_{A_i B_i} = 1.0$ while orthogonal, presumably independent, modes have $P_{A_i B_j} = 0$. With this value, we can estimate the difference between the results obtained from the transfer method (e.g., A) as compared to those from the full DFT calculation (B). Several similar pairs of modes can be identified due to their having close peak positions, similar intensities, and the same amide groups contributing to the computed displacements. All $P_{A_i B_j}$ values between possible pairs of modes from the transferred and full DFT computation for the 9-amide hairpin are given in Table 1. The result confirms that the pairs expected to be equivalent before applying the similarity measure show a high similarity measure especially if one views the amide I as two clusters of related modes, one computed for 1680–1700 cm^{-1} and another for 1714–1727 cm^{-1} . While the modes from amide groups in the strand are generally observed as coupled modes and spread over these clusters, the amide groups in the turn, in particular, that of the Aib, are found in the higher-frequency cluster. Furthermore each vibrational mode from the transfer method can be matched with a corresponding mode from the full DFT calculation. Except for two pairs, (1727, 1716 cm^{-1}) and (1709, 1714 cm^{-1}), where the first wavenumber is from the direct DFT and the second from the transfer method, each mode has a match with a P -value more than 0.8.

The fact that the matrix is not diagonal does indicate variation in the coupling of modes that can alter the ordering. In this case, it is the correlation of 1727 cm^{-1} with 1716 and 1714 cm^{-1} that shifts the other high P -values off the diagonal and

causes much of the shift of intensity between the higher-frequency modes in the two calculations. This means that the near-lying modes are mixed in different ways for these two calculations resulting in different eigenvalues, but the high P -values show that the mode content (atomic motion involved) is similar, with the exceptions noted above. The modes are otherwise in coupled pairs. The reversal of the two lowest-frequency modes has little impact on band shape due to their near degeneracy and large difference in their intensities. For high similarity pairs, the absolute frequency differences, $|\nu_{\alpha}^{\text{DFT}} - \nu_{\beta}^{\text{transfer}}|$, are only 1.2, 3.8, 1.6, 0.6, 3.1, 0.1, and 0.9 cm^{-1} , starting from the lowest-frequency pair.

The intensity ratios $D_{\alpha}^{\text{DFT}}/D_{\beta}^{\text{transfer}}$ vary more for these pairs being 0.5, 1.05, 0.89, 0.33, 0.36, 1.64, and 0.51, respectively, which might imply that the atomic polar tensors are more sensitive to details of the modes and influenced by longer-range interactions than the local force field and resulting eigenvalues. We conclude that the transfer method approximation preserves the general vibrational character, in particular similar frequencies, but may alter the dipole moments and the detailed band shape. This β -hairpin band shape pattern, characterized by the low-frequency intense peak and the exciton splitting between that and the high-frequency less intense peak, is consistently preserved in the transfer method, as discussed below.

Coupling parameters are important variables needed to understand isotope-labeled spectra and to interpret two-dimensional (2D) IR spectra.^{32,35,69} In Table 2 the coupling parameters calculated using the DFT and CSPT force fields are compared for the isotopically labeled positions in the hairpins, HGB1, HGB2, and HGB3. The differences in frequencies between the two calculations are within 3 cm^{-1} , but higher relative intensity differences, in particular for HGB3, are predicted. Overall, our results demonstrate that CSPT preserves important vibrational coupling patterns in isotope-labeled spectra including the phase relation between the coupled modes and the sign and qualitative magnitude of the splitting. Due to constrained optimization, these calculations are for peptides with the same geometry; if complete minimization were done, then the geometry would change, and the couplings could not be easily compared.

Amide I Simulation for HGB Conformations. Three structures, which we label I, II, and III (Figures 5a, 5b, and 5c, respectively) were chosen as examples for spectral simulations from molecular geometries generated by 300 K MD trajectories. We sought out variation rather than a statistical representation of a class of conformers. Structures I and II were sampled from among the folded states (Figure 2a), and structure III was chosen from conformations found after an unfolding event (which was in a longer trajectory and thus not seen in Figure 2a). In Figures 5a', 5b', and 5c', are illustrated amide I IR spectra computed using the CSPT method for these representative HGB structures. For the spectral simulation, the peptide sequences are reduced to all Ala except for the Aib-Gly turn. They encompass a well-folded state having all five hydrogen bonds formed (structure I, Figure 5a), an essentially folded structure having frayed ends and two hydrogen bonds (structure II, Figure 5b), and one of many possibilities for an extended, unfolded state (structure III, Figure 5c).

In structure I, despite having all possible hydrogen bonds, significant distortion from the conformation expected for a regular or even a twisted antiparallel β -sheet is seen for the terminal residues close to the ends. From our MD trajectories, structure II (Figure 5 b) appears to represent a more populated folded state with frayed termini, H_A and H_B weak or broken,

TABLE 1: Similarity Measures P for Modes Obtained by the Two Calculations for the 9-Amide β -Hairpin^a

ν_{DFT}	ν_{CSPT}								
	1722.3	1721.0	1716.3	1714.8	1711.4	1702.4	1695.0	1685.4	1683.7
1727.2	0.21	0.05	0.72	0.65	0.04	0.01	0.01	0.05	0.02
1721.4	0.97	0.11	0.18	0.12	0.07	0.05	0.02	0.03	0.02
1720.9	0.10	0.98	0.03	0.01	0.12	0.08	0.08	0.00	0.00
1714.5	0.06	0.13	0.33	0.30	0.83	0.17	0.19	0.06	0.15
1709.1	0.05	0.05	0.58	0.66	0.43	0.02	0.14	0.10	0.03
1701.8	0.04	0.07	0.05	0.05	0.26	0.86	0.41	0.05	0.08
1696.6	0.00	0.02	0.02	0.03	0.15	0.42	0.85	0.29	0.01
1687.5	0.03	0.02	0.01	0.07	0.12	0.16	0.07	0.51	0.83
1684.2	0.00	0.02	0.06	0.12	0.05	0.08	0.23	0.80	0.53

^a Frequencies in cm^{-1} . Bold elements ($P_{\text{DFT,CSPT},j}$ for k th DFT and j th CSPT mode) indicate the most similar pairs.

TABLE 2: Comparison of DFT and CSPT Spectral Parameters for Isotopically Labeled Peptides

	ν_{h}^a	ν_{l}	$\Delta\nu$	D_{h}^b	D_{l}	$D_{\text{h}}/D_{\text{l}}$
HGB1 DFT	1654.9 (−) ^c	1643.7 (+)	11.2	0.141	0.053	2.15
CSPT	1656.7 (−)	1642.9 (+)	13.8	0.136	0.084	1.62
HGB2 DFT	1663.2 (+)	1644.0 (−)	19.2	0.067	0.085	0.79
CSPT	1665.4 (+)	1643.3 (−)	22.1	0.085	0.114	0.75
HGB3 DFT	1654.8 (+)	1646.7 (−)	8.1	0.062	0.072	0.86
CSPT	1656.0 (n/a)	1644.2 (n/a)	11.8	0.087	0.062	1.4

^a ν_{h} and ν_{l} are frequencies (in cm^{-1}) for two isotope-labeled modes. Subscripts h and l represent the high- and low-frequency mode. ^b Dipole strength, D , of a mode in debye². ^c The phase relationships in a mode are given as + and − representing the symmetric and asymmetric coupling modes, respectively. The abbreviation n/a means that the coupling is too weak to be indicated.

and only the hydrogen bonds at H_{C} and H_{D} well-formed.⁶⁸ Structure III (Figure 5c) represents one possible unfolded state, which is clearly more complicated than the folded states since it has such a high configurational entropy.⁷⁰ Its turn still retains minimal structure as demonstrated by a hydrogen bond that forms between N–H of Gly7 and O=C of Glu4, which is encompassed in the [−3:2] 6-amide fragment. This structure represents an example of an unfolded state in which cross-strand interactions are broken but a minimal structure could be still be seen in the Aib-Gly region. While structure III is one of a broad ensemble of unfolded states, it provides a useful point of reference for generating comparisons of unfolded with folded state spectra.

Additionally we simulated a spectrum (Figure 6a′) for structure IV (Figure 6a), which is similar to that of structure II, being characterized by frayed ends, and is derived from the NMR structural parameters for this peptide in solution.⁷¹ This is compared to the spectrum (Figure 6b′)²³ of structure V (Figure 6b), an idealized hairpin modeled according to the crystal structure of a hairpin sequence in a well-formed β -sheet of the intestinal fatty acid binding protein (PDB code 1IFC).⁷² It has a modest twist of the strands and a quite regular hydrogen-bond structure, which is its main contrast to the folded structures I, II, and IV. This regular structure V, as reported previously, was modeled as a 13-amide hairpin, which was simulated by transfer of parameters computed for a pair of two strands, three amides each, by propagating it along the regular hairpin strands, and for a 5-amide turn model. For spectral modeling, the Asn in the turn was replaced by Ala, resulting in an Ala-Gly turn sequence for this idealized peptide. As suggested by a referee, experimentally obtained spectra are shown as dotted (low T hairpin) and dashed (high T “coil”) traces in Figure 5 by shifting and rescaling the experimental band shape to enhance overlap with the simulation at low T . Since these are vacuum calculations, the shift would need to differ at high T to account for

missing hydrogen bonds, but the unfolded bandwidths should be relevant.

Simulated amide I IR spectra (Figures 4–6) consistently show a characteristic band shape arising from the short antiparallel β -strand segment of folded β -hairpin states. These all have their most intense peak at the lowest frequency and an asymmetric overall amide I band shape that is mainly due to the dispersion (to higher frequencies) of weaker modes. In general, the less uniform the hairpin structure, the more the amide I intensity is dispersed over the other modes (compare Figure 6b with 6a and 5a and those with Figure 5b). Indeed, experimental spectral shapes are in good agreement with calculated spectra of the folded structures (Figures 5a′ and 6a′) and even the extended one (allowing for further shifting due to loss of hydrogen bonds) but are poor for the highly uniform (Figure 6b) structure V and for the partially unfolded (Figure 5b) structure II. The latter has to do with neglect of the larger number of externally hydrogen-bonded C=O groups (to solvent) in the vacuum calculation. The extended structure calculation has a relatively dense distribution of modes computed around 1710 cm^{-1} (which would correspond to an observed band at ~ 1640 – 1650 cm^{-1}) resulting in a more symmetric overall band shape than those of the hairpins. Such a change qualitatively matches what is observed in a hairpin-to-coil transformation.^{23,27}

Vibrational Coupling between Isotopically Labeled Amide Groups. CSPT Calculation. We have probed the correlation of structural change with site-specific coupling change and its consequent impact on the amide I IR spectra by simulating spectra for differently isotopically labeled (¹³C on the amide C=O) variants of the five configurations, structures I–V discussed above with our CSPT calculations. In Tables 3 and 4, calculated spectral parameters for the isotopic variants HBG1, HBG2, and HBG3 are summarized. HBG1 was labeled at −3 and 2 resulting in a larger 14-atom ring, and HBG2 at −3 and 4 and HBG3 at −1 and 2, respectively, forming smaller (10-atom) hydrogen-bonded rings (Figure 1). The results are summarized in Table 3, where the splitting of the two ¹³C=O modes ($\Delta\nu_{\text{h,l}}$) would be indicative of the coupling if the individual oscillators were degenerate. The diagonal FF contribution to the difference can be tested by calculation of the ¹³C=O modes for single-labeled species. The ratio of intensities $D_{\text{h}}/D_{\text{l}}$ indicates the sign of the coupling, which is opposite for HBG2 and HBG1. Ideally one would compare the splitting to observation, but in practice the weak component is not seen due to overlap with the stronger one. The ¹²C–¹³C shift (tabulated as $\Delta\nu_{12,13}$) is more easily measured and could be used to extract the experimental sign of the coupling. Finally the difference in ¹³C frequency for HBG1 and HBG2 is another useful observable for comparison with experiment.

While the extended structure III is, as would be expected, distinct from the others, the folded structures also show some

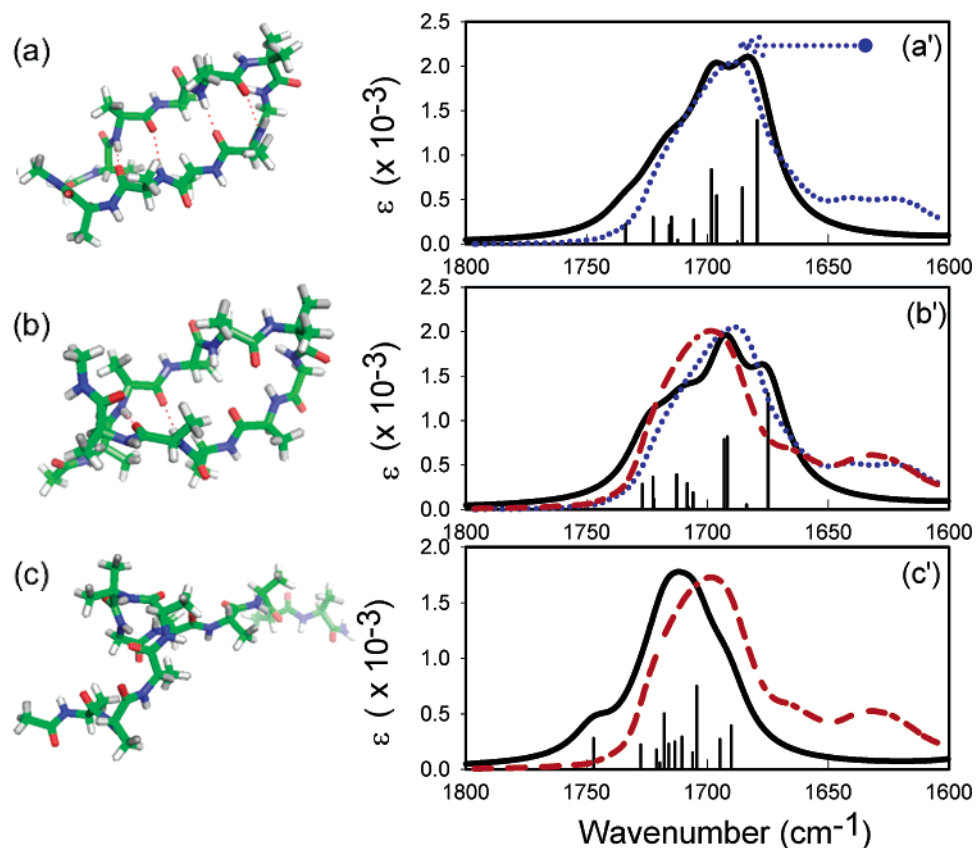


Figure 5. Amide I IR spectra of 11- or 12-amide β -hairpin models. Snapshot schematics of the backbone conformation of structures I, II, and III are shown in parts a, b, and c, respectively. The resulting simulated spectra are in parts a', b', and c', respectively. The dotted blue curve (parts a' and b') is the experimental low-temperature spectrum for the HBG peptide, shifted 55 cm^{-1} , as indicated by the blue arrow, and scaled to overlap the structure I prediction; the red dashed curve (parts b' and c') is the high-temperature result but with the same shift. Failure to overlap (part c') reflects the lack of hydrogen bonding to solvent in these vacuum calculations.

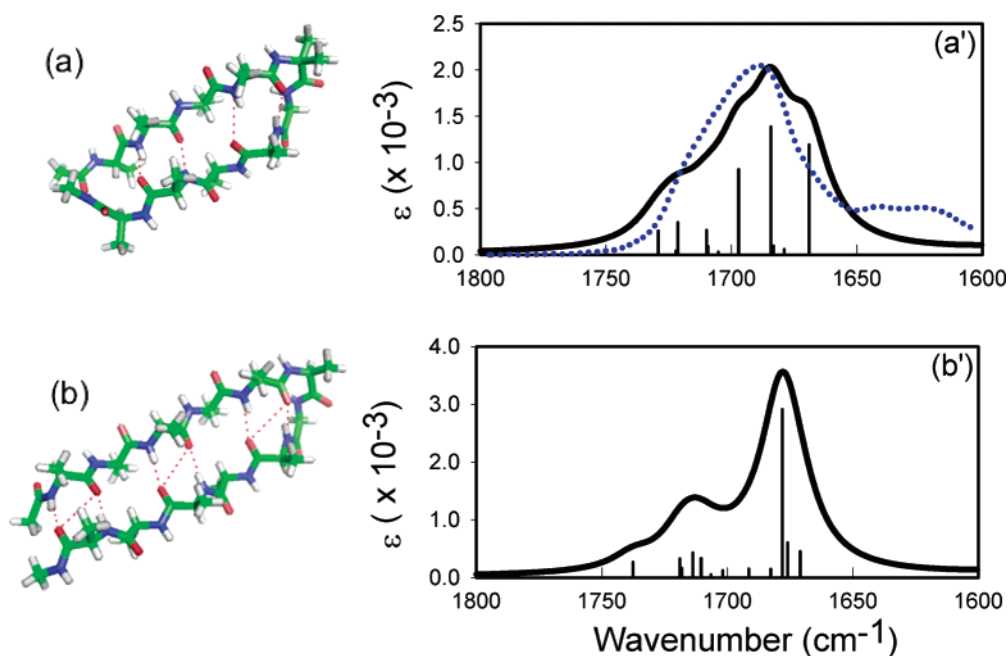


Figure 6. Amide I IR spectra for structures IV and V. Snapshot schematic of structure IV, obtained from an NMR structure, is shown in part a. Structure V, modeled from the crystal structure of IIFC is shown in part b. The corresponding spectra are in parts a' and b', respectively. The experimental spectrum (low T) of the HBG peptide is shifted and scaled as in Figure 5 and represented as the blue, dotted spectrum in part a'.

degree of coupling fluctuation. In particular, the variation in mean frequencies, ν_m , suggests that the localized residues have some nondegenerate nature, further reflected in the variation in splitting, $\Delta\nu_{h,i}$, as well as the relative intensity ratio, D_H/D_I . The

sign of the vibrational coupling is preserved, since all the folded structures generate an intense mode at a higher frequency for HBG1, while the intense mode in HBG2 is located at a lower frequency. Consequently, our results consistently predict the

TABLE 3: Calculated Spectral Parameters for Three Isotopically Labeled Peptide Variants

	HBG1 (-3,2) ^a				HBG2 (-3,4)				HBG3 (-1,2)				
	$\Delta\nu_{h,l}$ ^b	ν_m ^c	D_h/D_l ^d	$\Delta\nu_{12,13}$ ^e	$\Delta\nu$	ν_m	D_h/D_l	$\Delta\nu_{12,13}$	$\Delta\nu$	ν_m	D_h/D_l	$\Delta\nu_{12,13}$	$\Delta\nu_{\text{HBG1,HBG2}}$ ^f
I	14.4	1649.9	1.56	40.8	4.1	1642.5	0.05	57.6	11.6	1650.6	1.02	23.0	16.59
II	33.2	1652.2	1.26	22.6	8.2	1638.3	0.15	58.7	15.5	1661.9	0.42	21.8	34.53
III	11.8	1667.3	0.67	40.88	2.3	1672.0	1.69	31.8	14.3	1656.1	0.30	48.83	-11.8
IV	28.3	1642.0	1.15	27.4	12.5	1634.1	0.54	69.2	13.1	1648.8	1.06	14.5	28.27
V	8.2	1635.6	84.23	40.1	7.6	1635.6	0.01	45.0	15.2	1642.8	0.3	43	8
expt.			high	28			low	36					8

^a Two ¹³C-labeled amide groups. ^b Frequency difference between the high- and low-frequency labeled amide I modes, ν_h and ν_l . ^c Average frequency, $\nu_m = (\nu_h + \nu_l)/2$. ^d Intensity ratio for the two modes, D_h/D_l . ^e Frequency difference between the main ¹²C and ¹³C bands. Peak positions are determined according to the most intense modes. ^f Frequency difference, $\nu(\text{HBG1}) - \nu(\text{HBG2})$, between the most intense ¹³C bands in $\nu(\text{HBG1})$ and $\nu(\text{HBG2})$.

TABLE 4: Calculated Vibrational Coupling Constants for Three Isotopically Labeled Peptide Variants and Mode Frequencies in Single- or Double-Labeled Variants

	HBG1	HBG2	HBG3	HBG1	HBG2	HBG3	V3 ^b	V5	K8	I10
	HBG1	HBG2	HBG3	HBG1	HBG2	HBG3	V3 ^b	V5	K8	I10
	V ^a	V	V	(-3,2)	(-3,4)	(-1,2)	(-3)	(-1)	(2)	(4)
	V ^a	V	V	ν	ν	ν	ν	ν	ν	ν
I	2.7	1.9	0.8	1657.0 (-) ^c 1642.7 (+)	1644.6 (+) 1640.5 (-)	1656.4 (+) 1644.8 (-)	1643.1	1644.8	1656.3	1641.7
II	3.8	3.4	4.1	1668.8 (-) 1635.6 (+)	1642.4 (+) 1634.2 (-)	1669.6 (+) 1654.1 (-)	1635.7	1654.9	1668.0	1640.3
III	1.0	0	4.3	1673.2 (-) 1661.3 (+)	1673.1 (n/a) 1670.8 (n/a)	1663.3 (+) 1649.0 (-)	1673.1	1650.0	1661.4	1670.8
IV	3.9	1.6	0.8	1656.2 (-) 1627.8 (+)	1640.4 (+) 1627.9 (-)	1655.4 (-) 1642.3 (+)	1628.0	1655.3	1640.1	
V	4.1	3.8	2.8	1639.7 (-) 1631.5 (+)	1639.4 (+) 1631.8 (-)	1650.4 (+) 1635.1 (-)	1635.0	1649.7	1635.5	1635.4

^a Vibrational coupling constants are calculated by considering two isotope-labeled amide groups as coupled modes, and diagonal force constants are estimated by the frequencies obtained from the corresponding single-labeled hairpin. ^b Single-labeled variants. For example, V3 represents a variant in which Val3 is a ¹³C-labeled residue. ^c The phase relationships in a mode are given as + and - representing the symmetric and asymmetric coupling modes, respectively. The abbreviation n/a means that the coupling is too weak to be indicated.

¹³C=O band to be closer to the ¹²C=O band in HBG1 than in HBG2 for folded structures. Experimentally, the labeled band in HBG1 is observed at 1615 cm⁻¹, shifted down 28 cm⁻¹ from the ¹²C main band, and this is 8 cm⁻¹ higher in frequency than that of HBG2, which is in good agreement with our prediction.²³

Experimentally, the HBG3 variant generated a more complicated spectrum despite its formal similarity to HBG2 (since both label a smaller, 10-atom, hydrogen-bonded ring). HBG3 calculations show a nonconsistent pattern in coupling sign, relatively large fluctuation in the shift of the labeled peak from the ¹²C maximum, and relatively high mean frequencies in comparison to HBG1 and HBG2. These can generate more broadening in the labeled band as well as overlap with the main ¹²C band making the result harder to interpret. Indeed, the experimental results for HBG3 are complex and do not follow the HBG2 pattern, in qualitative agreement with the calculations.⁷³

TDC Calculation. Understanding structural fluctuation and its impact on in the isotope-labeled spectra requires that the results be averaged over a reasonable number of configurations. Since our MD simulation trajectories are extensive enough to contain sufficient dynamical information for the configuration space of interest, i.e., the compact, partially folded state, we examined folded structures developed in the trajectory with a simpler model of vibrational coupling, i.e., TDC. Quantitative accuracy may be degraded with such an empirical model, but it is expected to offer a reasonable interpretation of the variation in cross-strand coupling due to conformational fluctuation.^{41,74}

TDC between two amide C=O groups positioned as appropriate for our isotope-labeling variants, HBG1, HBG2, and

HBG3, were computed. Geometries used for the TDC calculations are taken from folded configurations sampled every 10 ps from 0 to 10 ns for the 300 K and 0 to 7 ns for the 400 K trajectories shown in Figure 2. Distributions of TDC coupling constants obtained for the HBG1, HBG2, and HBG3 labeling patterns from trajectories at two different temperatures, 300 and 400 K, are shown in Figures 7a and 7b, respectively.

As the temperature is increased, the distribution changes mostly reflect increased dynamical fluctuation in structure. For example, the appearance of the frayed ends at 400 K, which affect H_D , tends to center the HBG2 coupling constant distribution closer to zero. Despite similar structural fluctuations of H_B , H_C , and H_D at 300 K, HBG1 has a narrower coupling distribution than HBG2 and HBG3, which could reflect the larger distances between ¹³C=O positions typically found in this larger hydrogen-bonded ring structure, resulting in weaker, but on average predominantly negative, average dipolar interactions.

Coupling constant distributions with HBG2 and HBG3 are broader and can be used to interpret CSPT results in Table 3. For example, CSPT results with all of the folded state structures have a more intense lower-frequency mode for the HBG2 labeling pattern, which is consistent with the TDC-computed positive coupling constant (300 K distribution centered at 4–5 cm⁻¹). In the case of HBG3, CSPT calculations result in two different situations, one for the more regular structures, I and IV, and another for the more distorted ones (at the turn), II and V. Figure 7a shows both positive and negative contributions to HBG3 coupling, being on average approximately +2 cm⁻¹ for 300 K but ~0 cm⁻¹ for 400 K. The broad distribution for the

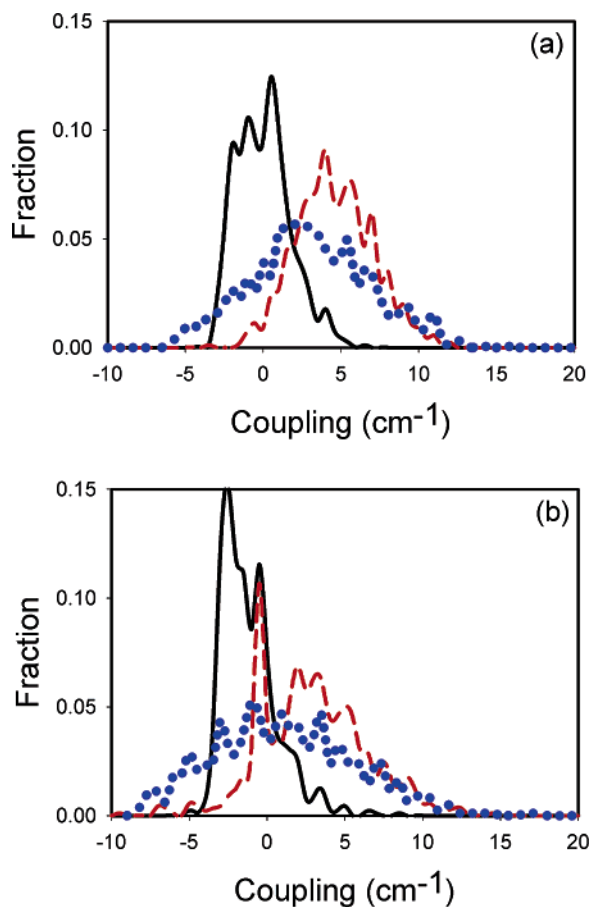


Figure 7. Normalized distributions of TDC coupling constants for HBG1, HBG2, and HBG3. The results obtained at 300 K are shown in part a, and the results at 400 K are in part b. The solid line (black) is for HBG1, the long dashed line (red) is for HBG2, and the dotted line (blue) is for HBG3, respectively. The employed TDC parameters are $2.73 \text{ D } \text{\AA}^{-1} \text{ amu}^{-1/2}$ for the magnitude of a transition dipole moment of the amide I mode, 10.0° for the angle between this moment and C=O, and $1.605 \text{ m dyn } \text{\AA}^{-1} \text{ amu}^{-1}$ for the diagonal force constant.

HBG3 labeling, even as compared to HBG2, would arise from dynamical fluctuation at H_A as well as more fluctuation in the turn residues. HBG1 distributions suggest that the structural variations could result in positive as well as (lower probability) negative values.

Despite the broad distributions, these results on average predict the relative peak positions seen between HBG1 and HBG2 in our experimental spectra. Due to its negative coupling constant, the HBG1 ¹³C=O group should have less shift from the ¹²C=O group than should HBG2, because for HBG1 the higher-frequency component will be the more intense and the opposite will be true for HBG2. These TDC-simulated spectra, using the same parameters as for Figure 7, are illustrated in Figure 8a for the 300 K trajectory and compared with the experimental ¹³C=O amide I IR for HBG1 and HBG2 in Figure 8c.²³ Since the central frequency is arbitrary in these TDC-computed spectra, that was chosen to overlap the experimental HBG1 peak position. The spread of the intensity distributions (line widths and average separations) in these predicted spectra are sensitive to the parameters used for the TDC calculations, as can be seen by comparison to Figure 8b, where a different set of parameters from Torii are used.⁵⁴ Clearly the original (Figure 8a) set better reflects experimentally observed spectral patterns. However the widths seen experimentally do seem broader than those computed with this dynamics-based approach. We have previously shown that the fluctuation of water can

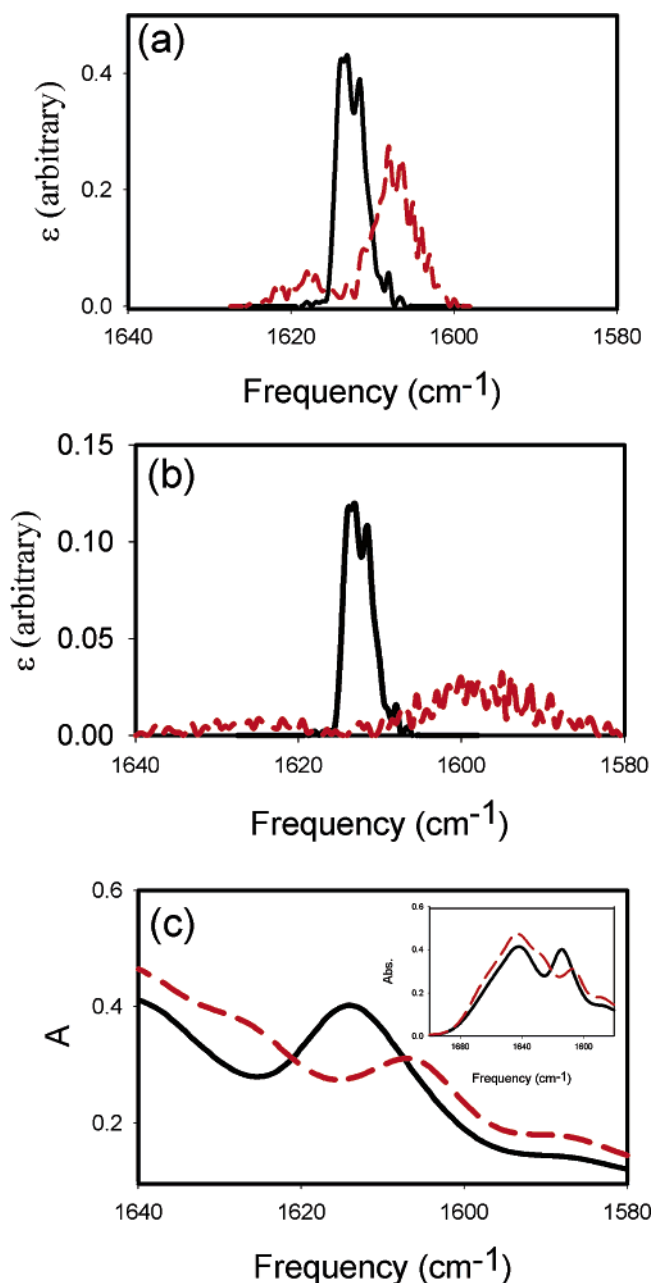


Figure 8. TDC-simulated spectra for HBG1 and HBG2 variants. (a) Spectra obtained with the parameter set that was used for calculations in Figure 7. (b) Spectra obtained with the alternate parameter set: $3.985 \text{ D } \text{\AA}^{-1} \text{ amu}^{-1/2}$ for the magnitude of a transition dipole moment of the amide I mode, 15.5° for the angle between this moment and C=O, and $1.605 \text{ m dyn } \text{\AA}^{-1} \text{ amu}^{-1}$ for the diagonal force constant. The solid lines (black) are for HBG1, and the long dashed lines (red) are for HBG2. Experimentally obtained spectra are shown in part c.²³ TDC-calculated frequencies are shifted to the peak position of the experimental HBG1 spectra, and units for absorbance for the calculated spectra are arbitrary.

lead to a large dispersion of frequencies, which may be a contributor here as well.^{14,75}

Discussion

Segmentation Test. In this study we simulated the infrared spectra of β -hairpins of various conformations using the CSPT model to transfer parameters from DFT calculations on small subsystems. Two important issues for the choice of subsystems are the sizes of the segments and the overlap between them. The segment should be large enough to encompass the most

important vibrational coupling mechanisms, e.g., short-range mechanical interactions through covalent or hydrogen bonds and the strongest through-space electrostatic couplings. Long-range interactions beyond the segment should be negligible so that CSPT-computed spectral properties can satisfactorily mimic the results of the full DFT calculation. Further correction for long-range electrostatic interactions might then be obtained empirically with the TDC model if needed.⁷⁶ Second, a sufficient overlap between segments is necessary to avoid artificial end effects that can arise if properties from a terminal segment are mapped onto a sequential amide group. For example, in Ac-(Ala)_N-NMe, Ala residues next to -Ac and -NMe have spectral properties (FF, APT, and AAT) different from those of central or sequential amide groups connected forward and back to Ala residues. Our recent tests of this issue with a β -hairpin structure taken from a Trpzip peptide³¹ found that an overlap of two amide groups between fragments yielded the best match with a full DFT calculation, but a one-amide overlap was qualitatively comparable. On the basis of this, for our CSPT calculation, we used a one-amide overlap between the turn segment and the strand segment. For the amide I mode, these are in overall agreement with a full DFT calculation for a 9-amide hairpin (Figure 4).

Our new substructure scheme has variably sized segments as compared to previous CSPT implementations with regular peptide structures.^{39,48,74,77} This irregularity can affect the diagonal FF and perhaps can lead to unrealistic perturbations and end effects being incorporated into the diagonal FF elements. The results above demonstrate that our heterogeneous segmentation, i.e., into a 5-amide turn fragment and 6-amide fragment composed of two strands, is a reasonable choice for the substructure scheme for our β -hairpin model peptide, if we are seeking to represent the major amide I spectral features.

Origin of Characteristic Band Shape for β -Hairpin Peptides. Amide I IR spectra of small β -hairpin peptides have characteristics that are distinctively different from helical or coil-like peptides. The β -sheet in globular proteins has a variable degree of right-handed twist, typically less than that seen for an isolated hairpin peptide. Experimental protein β -sheet spectra are characterized by an intense low-frequency peak at ~ 1625 – 1640 cm^{-1} with a high-frequency, weak component at ~ 1675 – 1695 cm^{-1} , resulting in an asymmetric band shape. Many β -hairpin peptide models including HBG and the original Gellman sequence stabilized by D-Pro-Gly show an asymmetric band shape with an intense low-frequency peak at ~ 1635 cm^{-1} , well below that typical of helical or random coil peptides and above that expected for an extended, flat β -sheet.^{23,27,30,31,34,35,37} Then one should ask, what structural properties are relevant to such characteristic amide I IR spectra?

Previous studies attempted to understand the β -turn contribution by examining the correlation of IR or VCD spectra with turn geometries.^{27,29,78} For example, it was found that in peptides with a D-Pro-Gly turn sequence, a characteristic low-frequency amide I component could be assigned to the Xxx-D-Pro linkage based on theoretical and experimental correlation.^{27,79} Similarly, most turn geometries develop a high-frequency (~ 1660 – 70 cm^{-1}) transition due to the amide C=O pointing out into solution that is not well-coupled to the remaining amide residues.²⁷ However, prediction of the turn geometry based on spectra is still a challenge. While our MD simulation indicated that an Aib-Gly turn sequence in HBG adopts type I' turn geometry and the previously studied D-Pro-Gly turn sequence peptide model can be type I' or type II',^{56,68,79,80} the spectral signatures for such structural differences are not obvious in the

IR spectra. While VCD may be a useful tool for discriminating "mirror turn" geometries from "common turn" geometries,^{13,29,81} predicting a specific type of the turn is hampered by the intrinsic low resolution of vibrational spectra. Growing evidence suggests that the contribution from the turn in amide I spectra for larger hairpin peptides could have little impact in generating a characteristic amide I band shape, in contrast to the strand contribution. Turns, particularly tight turn sequences such as Aib-Gly or D-Pro-Gly, lack long-range structural character, which can yield a characteristic repeated coupling pattern, instead resulting in local, nondegenerate modes that are dispersed by dynamical fluctuation. As the impact of hydrogen bonds in vibrational properties is significant,^{12,18,20,55,82,83} different spectral patterns result in segments with and without a hydrogen bond. Our MD results showed that even in the folded state a transient hydrogen bond between O of Val5 and N-H of Gly7 can be formed as the turn structure fluctuates. In addition, the amide group of Val5 is, at least partially, solvent-accessible (Figure 3). All combined, it is unlikely that spectral contributions from the turn generate consistent properties in terms of peak frequencies and vibrational coupling.

However, our results suggest that the structural properties of the strand and associated spectral properties are the origin of the characteristic amide I IR band. MD simulation results indicated significant fraying of end residues at positions 5 and -5 over the lifetime of the folded state, which has been also observed with other small β -hairpin peptides.⁶⁵ These frayed amide residues are also exposed to water. Such aspects lead to the assumption that the spectral contribution from the end groups could be diffuse and nonspecific (Figures 4 and 5a'). In contrast, cross-strand amide groups at H_B, H_C, and H_D are relatively immune to hydration effects and show stable structural characteristics, despite conformational fluctuation within the various folded states.

The remaining question is whether such a dynamically fluctuating structural motif in the strand could generate the characteristic band shape of β -hairpin peptides. Although the characteristic exciton split amide I IR band shape pattern of the antiparallel β -sheet is only developed for relatively long multistrand models,⁷⁷ the dominant interactions are intrinsic to our short two-strand models used for hairpin simulation but here result in less splitting and broader bands due to conformational nonuniformity of the coupled residues in the structure. This short-range coupling pattern is unique in comparison to secondary structures such as α -, 3_{10} -, or 3_1 -helices. As found with our previous DFT calculations for various " $a \times b$ " β -sheet segments (where a is the number of strands and b the number of amides in each strand) encompassing 1×3 , 2×3 , 3×3 , 2×6 , and 1×7 structures as well as different degrees of twist,^{74,76,77,84} splitting of amide I and partitioning of intensity into the lowest-frequency mode are observed with minimal models such as the 2×3 . The intense mode typically has an out-of-phase in-strand vibrational motion for $(i, i + 1)$ and in-phase and out-of-phase cross-strand coupled motion for (i, j) and $(i, j + 1)$ located in proximity, where i represents an amide, $i + 1$ the nearest in-strand neighbor, and j represents the closest cross-strand amide group. Early studies on vibrational coupling in β -sheet models showed these interactions, labeled as D_{10} , D_{01} , and D_{11} ,^{6,63,85} to be the source of the characteristic low-frequency intense modes that are a consequence of the resulting exciton splitting. These local couplings are the most prominent spectral characteristic found among β -sheet models and have been utilized to model experimentally obtained spectra of β -sheet structures. However, coupling patterns observed with various structural models where

spectra were simulated with DFT were found to be more complicated. Heterogeneity in local coupling interactions was observed with full QM calculations, which can be associated with heterogeneity in diagonal force constants, i.e., nondegeneracy. Regular structures give rise to an intense low-frequency mode delocalized over the central residues of the structure. However, as distortion increases and the local modes become more nondegenerate, the intensity of this band is dispersed over several modes that are then more localized. This evolution in mode character leads to broadening of the pattern and less exciton splitting of the upper and lower energy transitions, but the characteristic β -sheet profile can still be detected and is distinct from other structures.

By contrast, the extended structure III yields spectra (Figure 5c') with vibrational patterns uniquely different from the folded β -hairpin structures. Its lack of dispersion results in a congestion of modes in the middle of the amide I band. Since this configuration has no cross-strand interactions, its dispersion must result from only in-strand coupling, which being irregular, does not yield the characteristic β -hairpin asymmetric, dispersed band.

Recently, by means of 2D IR, in dispersed vibrational echo (DVE) spectra of a Trpzip2 β -hairpin peptide, it was also determined experimentally that the weak high-frequency and intense low-frequency amide I modes originated from vibrational coupling as opposed to a diagonal FF effect.³⁵ Our results demonstrate that the short antiparallel strand motif could generate such a coupling despite any intrinsic nondegeneracy associated with the local structure heterogeneity.

Conformational Fluctuation and Its Impact on Vibrational Coupling. Conformations of the peptide obtained from our MD simulations represent the dynamically evolving system interacting with surrounding explicit water molecules within a classical force field description. Information such as the structural fluctuation, hydration structure, and distributions of structural parameters related to dipolar coupling calculations were extracted from them.

In Table 3, the impact of conformational variation on the spectra of vibrationally coupled ^{13}C -labeled residues is demonstrated by each configuration and labeling pattern generating mode splittings that vary substantially in magnitude. If these apparent splittings are analyzed to account for diagonal nondegeneracies in the coupled modes (using single-labeled models), then the actual coupling constants (especially for the folded structures I, II, IV, and V) are quite similar, as shown in Table 4, particularly for HBG1 and HBG2. These vibrational couplings give rise to a consistent pattern in good agreement with experimental spectra; the peak frequency of the ^{13}C -shifted band in HBG1 is higher than that in HBG2, primarily due to the sign change in the coupling for the two labeling patterns. This pattern is also maintained through the MD trajectory, as simulated with TDC modeling (see discussion below).

It is also useful to initially discuss the underlying vibrational coupling mechanism in the regular hairpin, structure V. Relatively simple patterns for HBG1 and HBG2 indicate the existence of strong vibrational coupling between two near-degenerate ^{13}C amide modes but weaker coupling results in HBG3. Evaluation of the mean frequencies and the intensity ratio points to a nondegenerate contribution in HBG3. HBG1 and HBG2 have similar mean frequencies and components that have ~ 100 times differences in intensities, meaning that the observed ^{13}C band corresponds to one component mode. The splitting between the two isotope-labeled modes is governed by the off-diagonal coupling, and thus its size represents the strength of the coupling. The opposite sign of the coupling in

HBG1 and HBG2 results in the former having an intense high-frequency mode while the latter has an intense low-frequency mode. In comparison to structure V, the distortions in I, II, and IV provide insight as to the role of conformational fluctuation in vibrational spectral properties. These distorted structures have more apparent nondegeneracy in their diagonal force fields (Table 3) as indicated by the variation of the mean frequencies as well as the splitting. Due to nondegeneracy, vibrational coupling impact on the two ^{13}C modes becomes weaker, and mixing with neighboring ^{12}C modes is also observed. Nonetheless, the sign of the coupling is maintained, which generates the observed relative intensity pattern for HBG1 and HBG2.

The actual splitting computed for the labeled C=O bands in HBG1 and HBG2 is difficult to verify experimentally, due to the difference in intensity of the in-phase and out-of-phase components and to spectral overlap. Since these labeled C=O groups are fairly shielded from the solvent, perhaps conformational fluctuation, whose influence is underestimated with the small number of CSPT-evaluated configurations reported here, might be the problem in matching the experimental results. While the vibrational coupling constant will be somewhat sensitive to the structure, our empirical (TDC) evaluation of the effect on coupling of the large number of conformations in the MD indicates that the qualitative pattern prevails.

If we are willing to accept the approximation of limiting the role of the diagonal terms to the local FF of labeled amide C=O oscillators, then TDC is an attractive approach for determining off-diagonal contributions, particularly for cross-strand interactions. We applied a TDC approximation between two ^{13}C =O modes in cross-strand isotope-labeled variants for folded conformations sampled along our MD trajectories. Coupling between ^{12}C modes and ^{13}C modes was neglected to focus on the correlation of structural fluctuation and transition-dipole-mediated interactions. While the TDC approximation does not adequately represent vibrationally coupled interaction between amide I modes of covalently bound nearest neighbor residues,^{74,86} it has been proposed as an effective way to describe an off-diagonal interaction between amide groups moderately separated in the sequence or for interstrand interactions such as in β -sheets.^{6,76}

Our results with the TDC approximation can be summarized in terms of the broadening of the coupling constants resulting from different amounts of local fluctuation among the isotope variants, as shown in Figure 7. These give rise to TDC-simulated spectral patterns that directly reflect the coupling constant distributions; in other words, HBG1 has a band at a higher frequency from the zero position (unperturbed diagonal frequency), and HBG2 is substantially lower. The bandwidths (from summing the contributions of uniformly sampled structures in the trajectory) are such that they would overlap slightly but be clearly distinguishable, reflecting experimental observations. The widths suggest that coupling constants vary as configurations fluctuate, but the impact of structural environments in each isotope variant generates unique intensity distributions. Despite the variations in coupling constants, the band position is consistent enough to represent the experimental pattern, HBG1 higher and HBG2 lower in frequency. Again, HBG3 gives the broadest distribution, and our results demonstrate that significant modulation of off-diagonal coupling strength associated with thermal fluctuation of structure could be one source of such a complicated coupling pattern of HBG3.

Conclusions

Dynamical information from MD simulations was utilized for spectral simulation of the 12-residue β -hairpin peptide

stabilized by an Aib-Gly turn sequence. The impact of structural variations, intrinsically associated with conformational fluctuation during the unfolding–refolding dynamics of the peptide in explicit water, on the amide I IR spectra was examined. By use of CSPT calculations, implemented with a substructure scheme, spectra were obtained for configurations sampled from a MD trajectory. While our current implementation might miss some important aspects of the solvent that differently influence exposed amide groups and buried amide groups, we suggest that the calculated (vacuum) spectra can provide a consistent description of the origin of amide I IR spectra for a β -hairpin structure. A major limitation in testing the model versus real data is the relative lack of detail in the amide I IR band shape. We have addressed this by site-specific isotopic labeling experiments²³ and theoretical simulation, and perhaps future studies will use 2D IR results to enhance resolution and identification of the vibrational components.³⁵ The characteristic amide I band line shape of a small β -hairpin peptide dominantly arises from the amide groups located in the short antiparallel β -strand comprised of hydrogen bonds at H_B , H_C , and H_D . Calculated spectra revealed variations in vibrational coupling patterns as a different configuration was used and thus demonstrated the impact of conformational change in vibrational couplings in ¹³C isotope-labeled variants. To grasp the overall character in variation of vibrational couplings among possible conformations, the TDC approximation was applied for the number of configurations sampled from MD trajectories. Our results are in good agreement with experimental spectra reported for the β -hairpins previously, in terms of the characteristic coupling pattern between HBG2 and HBG1, and also indicate that complicated factors led to the band profile observed with HBG3.

Acknowledgment. This work was supported in part by a grant from the National Science Foundation (CHE03-16014). Some of its development was undertaken while one author (T.A.K.) was supported by a Guggenheim Fellowship.

References and Notes

- Finley, J. W.; Stephens, P. J. *J. Mol. Struct. (THEOCHEM)* **1995**, 357, 225.
- Devlin, F. J.; Finley, J. W.; Stephens, P. J.; Frisch, M. J. *J. Phys. Chem.* **1995**, 99, 16883.
- Devlin, F. J.; Stephens, P. J.; Cheeseman, J. R.; Frisch, M. J. *J. Phys. Chem.* **1997**, 101, 9912.
- Stephens, P. J.; Ashvar, C. S.; Devlin, F. J.; Cheeseman, J. R.; Frisch, M. J. *Mol. Phys.* **1996**, 89, 579.
- Barth, A.; Zscherp, C. *Q. Rev. Biophys.* **2002**, 35, 369.
- Krimm, S.; Bandekar, J. *Adv. Protein Chem.* **1986**, 38, 181.
- Woutersen, S.; Hamm, P. *J. Phys.: Condens. Matter* **2002**, 14, R1035.
- McQuirrie, D. A. *Statistical Mechanics*; Harper & Row: New York, 1976.
- Lawrence, C. P.; Skinner, J. L. *J. Chem. Phys.* **2002**, 117, 8847.
- Oxtoby, D. W.; Levesque, D.; Weis, J.-J. *J. Chem. Phys.* **1978**, 68, 5528.
- Keyes, T.; Kim, J. *J. Chem. Phys.* **2005**, 122, 244502.
- Kubelka, J.; Keiderling, T. A. *J. Phys. Chem. A* **2001**, 105, 10922.
- Kubelka, J.; Silva, R. A. G. D.; Bour, P.; Decatur, S. M.; Keiderling, T. A. In *Chirality: Physical Chemistry*; Hicks, J. M., Ed.; ACS Symposium Series 810; American Chemical Society: Washington, DC, 2002; p 50.
- Bour, P.; Keiderling, T. A. *J. Chem. Phys.* **2003**, 119, 11253.
- Kwac, K.; Cho, M. *J. Chem. Phys.* **2003**, 119, 2247.
- Schmidt, S. A.; Corcelli, S. A.; Skinner, J. L. *J. Chem. Phys.* **2004**, 121, 8887.
- Thompson, W. H. *J. Chem. Phys.* **2003**, 118, 1059.
- Besley, N. A. *J. Phys. Chem. A* **2004**, 108, 10794.
- Fecko, C. J.; Eaves, J. D.; Lopano, J. J.; Tokmakoff, A.; Geissler, P. L. *Science* **2003**, 301, 1698.
- Kubelka, J.; Huang, R.; Keiderling, T. A. *J. Phys. Chem. B* **2005**, 109, 8231.
- Li, S.; Schmidt, S. A.; Corcelli, S. A.; Lawrence, C. P.; Skinner, J. L. *J. Chem. Phys.* **2006**, 124, 204110.
- Cho, M. *J. Chem. Phys.* **2003**, 118, 3480.
- Setnicka, V.; Huang, R.; Thomas, C. L.; Etienne, M. A.; Kubelka, J.; Hammer, R. P.; Keiderling, T. A. *J. Am. Chem. Soc.* **2005**, 127, 4992.
- Gellman, S. H. *Curr. Opin. Struct. Biol.* **1992**, 2, 717.
- Griffiths-Jones, S. R.; Maynard, A. J.; Searle, M. S. *J. Mol. Biol.* **1999**, 292, 1051.
- de Alba, E.; Jimenez, M. A.; Rico, M.; Nieto, J. L. *Folding Des.* **1996**, 1, 133.
- Hilario, J.; Kubelka, J.; Keiderling, T. A. *J. Am. Chem. Soc.* **2003**, 125, 7562.
- Galzitskaya, O. V.; Higo, J.; Finkelstein, A. V. *Curr. Protein Pept. Sci.* **2002**, 3, 191.
- Polavarapu, P. L.; Zhao, C.; Das, C.; Balam, P. *J. Am. Chem. Soc.* **2000**, 122, 8228.
- Du, D.; Zhu, Y.; Huang, C.; Gai, F. *Proc. Natl. Acad. Sci. U.S.A.* **2004**, 101, 15915.
- Bour, P.; Keiderling, T. A. *J. Phys. Chem. B* **2005**, 109, 23687.
- Cheatum, C. M.; Tokmakoff, A. *J. Chem. Phys.* **2004**, 120, 8201.
- Dyer, R. B.; Maness, S. J.; Peterson, E. S.; Franzen, S.; Fesinmeyer, R. M.; Andersen, N. H. *Biochemistry* **2004**, 43, 11560.
- Yang, W.-Y.; Pitera, J. W.; Swope, W. C.; Gruebele, M. *J. Mol. Biol.* **2004**, 336, 241.
- Smith, A. W.; Chung, H. S.; Ganim, Z.; Tokmakoff, A. *J. Phys. Chem. B* **2005**, 109, 17025.
- Snow, C. D.; Qiu, L.; Du, D.; Gai, F.; Hagen, S. J.; Pande, V. S. *Proc. Natl. Acad. Sci. U.S.A.* **2004**, 101, 4077.
- Wang, J.; Chen, J.; Hochstrasser, R. M. *J. Phys. Chem. B* **2006**, 110, 7545.
- Dyer, R. B.; Maness, S. J.; Franzen, S.; Fesinmeyer, R. M.; Olsen, K. A.; Andersen, N. H. *Biochemistry* **2005**, 44, 10406.
- Silva, R. A. G. D.; Kubelka, J.; Decatur, S. M.; Bour, P.; Keiderling, T. A. *Proc. Natl. Acad. Sci. U.S.A.* **2000**, 97, 8318.
- Decatur, S. M.; Antonic, J. *J. Am. Chem. Soc.* **1999**, 121, 11914.
- Paul, C.; Wang, J.; Wimley, W. C.; Hochstrasser, R. M.; Axelsen, P. H. *J. Am. Chem. Soc.* **2004**, 126, 5843.
- Brauner, J. W.; Dugan, C.; Mendelsohn, R. *J. Am. Chem. Soc.* **2000**, 122, 677.
- Kubelka, J.; Keiderling, T. A. *J. Am. Chem. Soc.* **2001**, 123, 6142.
- Halverson, K.; Sucholeiki, I.; Ashburn, T. T.; Lansbury, P. T. *J. Am. Chem. Soc.* **1991**, 113, 6701.
- Fang, C.; Wang, J.; Charney, A. K.; Barber-Armstrong, W.; Smith, A. B., III.; Decatur, S. M.; Hochstrasser, R. M. *Chem. Phys. Lett.* **2003**, 382, 586.
- Harris, P. I.; Robillard, G. T.; van Dijk, A. A.; Chapman, D. *Biochemistry* **1992**, 31, 6279.
- Ludlam, C. F. C.; Arkin, I. T.; Liu, X. M.; Rothman, M. S.; Rath, P.; Aimoto, S.; Smith, S. O.; Engelman, D. M.; Rothschild, K. J. *Biophys. J.* **1996**, 70, 1728.
- Huang, R.; Kubelka, J.; Barber-Armstrong, W.; Silva, R. A. G. D.; Decatur, S. M.; Keiderling, T. A. *J. Am. Chem. Soc.* **2004**, 126, 2346.
- Fesinmeyer, R. M.; Peterson, E. S.; Dyer, R. B.; Andersen, N. H. *Protein Sci.* **2005**, 14, 2324.
- Gnanakaran, S.; Hochstrasser, R. M.; García, A. E. *Proc. Natl. Acad. Sci. U.S.A.* **2004**, 101, 9229.
- Walsh, S. T. R.; Cheng, R. P.; Wright, W. W.; Alonso, D. O. V.; Daggett, V.; Vanderkooi, J. M.; DeGrado, W. F. *Protein Sci.* **2003**, 12, 520.
- Ramajo, A. P.; Petty, S. A.; Starzyk, A.; Decatur, S. M.; Volk, M. *J. Am. Chem. Soc.* **2005**, 127, 13784.
- Starzyk, A.; Barber-Armstrong, W.; Sridharan, M.; M. Decatur, S. M. *Biochemistry* **2005**, 44, 369.
- Torii, H. *J. Phys. Chem. A* **2004**, 108, 7272.
- Torii, H.; Tatsumi, T.; Tasumi, M. *J. Raman Spectrosc.* **1998**, 29, 537.
- Syud, F. A.; Stanger, H. E.; Gellman, S. H. *J. Am. Chem. Soc.* **2001**, 123, 8667.
- Lindahl, E.; Hess, B.; van der Spoel, D. *J. Mol. Model.* **2001**, 7, 306.
- Jorgensen, W.; Maxwell, D. S.; Tirado-Rives, J. *J. Am. Chem. Soc.* **1996**, 118, 11225.
- Berendsen, H. J. C.; Postma, J. P. M.; van Gunsteren, W. F.; Hermans, J. *Intermolecular Forces*. In *Intermolecular Forces*; Pullman, B., Ed.; Reidel: Dordrecht, The Netherlands, 1981; p 331.
- Bour, P.; Sopkova, J.; Bednarova, L.; Malon, P.; Keiderling, T. A. *J. Comput. Chem.* **1997**, 18, 646.
- Choi, J. H.; Cho, M. *J. Chem. Phys.* **2004**, 120, 4383.
- Frisch, M. J.; Trucks, G. W.; Schlegel, H. B.; Scuseria, G. E.; Robb, M. A.; Cheeseman, J. R.; Montgomery, J. A., Jr.; Vreven, T.; Kudin, K. N.; Burant, J. C.; Millam, J. M.; Iyengar, S. S.; Tomasi, J.; Barone, V.; Mennucci, B.; Cossi, M.; Scalmani, G.; Rega, N.; Petersson, G. A.; Nakatsuji, H.; Hada, M.; Ehara, M.; Toyota, K.; Fukuda, R.; Hasegawa, J.;

- Ishida, M.; Nakajima, T.; Honda, Y.; Kitao, O.; Nakai, H.; Klene, M.; Li, X.; Knox, J. E.; Hratchian, H. P.; Cross, J. B.; Bakken, V.; Adamo, C.; Jaramillo, J.; Gomperts, R.; Stratmann, R. E.; Yazyev, O.; Austin, A. J.; Cammi, R.; Pomelli, C.; Ochterski, J. W.; Ayala, P. Y.; Morokuma, K.; Voth, G. A.; Salvador, P.; Dannenberg, J. J.; Zakrzewski, V. G.; Dapprich, S.; Daniels, A. D.; Strain, M. C.; Farkas, O.; Malick, D. K.; Rabuck, A. D.; Raghavachari, K.; Foresman, J. B.; Ortiz, J. V.; Cui, Q.; Baboul, A. G.; Clifford, S.; Cioslowski, J.; Stefanov, B. B.; Liu, G.; Liashenko, A.; Piskorz, P.; Komaromi, I.; Martin, R. L.; Fox, D. J.; Keith, T.; Al-Laham, M. A.; Peng, C. Y.; Nanayakkara, A.; Challacombe, M.; Gill, P. M. W.; Johnson, B.; Chen, W.; Wong, M. W.; Gonzalez, C.; Pople, J. A. *Gaussian 03*, revision C.02; Gaussian, Inc.: Wallingford, CT, 2004.
- (63) Moore, W. H.; Krimm, S. *Proc. Natl. Acad. Sci. U.S.A.* **1975**, *72*, 4933.
- (64) Torii, H.; Tasumi, M. *J. Chem. Phys.* **1992**, *96*, 3379.
- (65) Bolhuis, P. G. *Proc. Natl. Acad. Sci. U.S.A.* **2003**, *100*, 12129.
- (66) Zhang, J.; Qin, M.; Wang, W. *Proteins: Struct., Funct., Bioinf.* **2006**, *62*, 672.
- (67) Zhou, R.; Berne, B. J. *Proc. Natl. Acad. Sci. U.S.A.* **2002**, *99*, 12777.
- (68) Kim, J.; Keiderling, T. A. Unpublished work.
- (69) Hahn, S.; Kim, S.; Lee, C.; Cho, M. *J. Chem. Phys.* **2005**, *123*, 084905.
- (70) Marianayagam, N. J.; Fawzi, N. L.; Head-Gordon, T. *Proc. Natl. Acad. Sci. U.S.A.* **2005**, *102*, 16684.
- (71) Hammer, R. P. Unpublished work.
- (72) Scapin, G.; Gordon, J. I.; Sacchettini, J. C. *J. Biol. Chem.* **1992**, *267*, 4253.
- (73) Huang, R. Unpublished work, 2006.
- (74) Bour, P.; Keiderling, T. A. *J. Phys. Chem. B* **2005**, *109*, 5348.
- (75) Bour, P.; Michalik, D.; Kapitan, J. *J. Chem. Phys.* **2005**, *122*, 144501.
- (76) Kim, J.; Keiderling, T. A. Unpublished work.
- (77) Kubelka, J.; Keiderling, T. A. *J. Am. Chem. Soc.* **2001**, *123*, 12048.
- (78) Vass, E.; Hollosi, M.; Besson, F.; Buchet, R. *Chem. Rev.* **2003**, *103*, 1917.
- (79) Hilario, J.; Kubelka, J.; Syud, F. A.; Gellman, S. H.; Keiderling, T. A. *Biopolymers* **2002**, *67*, 233.
- (80) Stanger, H. E.; Gellman, S. H. *J. Am. Chem. Soc.* **1998**, *120*, 4236.
- (81) Kim, J.; Keiderling, T. A. Unpublished work.
- (82) Guo, H.; Karplus, M. *J. Phys. Chem.* **1992**, *96*, 7273.
- (83) Jalkanen, K. J.; Jurgensen, V. W.; Claussen, A.; Rahim, A.; Jensen, G. M.; Wade, R. C.; Nardi, F.; Jung, C.; Degtyarenko, I. M.; Nieminen, R. M.; Herrmann, F.; Knapp-Mohammady, M.; Niehaus, T. A.; Frimand, K.; Suhai, S. *Int. J. Quantum Chem.* **2006**, *106*, 1160.
- (84) Bour, P.; Keiderling, T. A. *J. Mol. Struct. (THEOCHEM)* **2004**, *675*, 95.
- (85) Miyazawa, T.; Blout, E. R. *J. Am. Chem. Soc.* **1961**, *83*, 712.
- (86) Kubelka, J.; Kim, J.; Bour, P.; Keiderling, T. A. *Vib. Spectrosc.* **2006**, *42*, 63.